Impact of nucleon-nucleon bremsstrahlung rates beyond one-pion exchange

A. Bartl, R. Bollig, H.-T. Janka, and A. Schwenk

Phys. Rev. D **94**, 083009 — Published 28 October 2016

DOI: 10.1103/PhysRevD.94.083009

Impact of Nucleon-Nucleon Bremsstrahlung Rates Beyond One-Pion Exchange

A. Bartl,[1,2] R. Bollig,[3,4] H.-T. Janka,[3] and A. Schwenk[1,2,5]

[1] *Institut für Kernphysik, Technische Universität Darmstadt, 64289 Darmstadt, Germany*
[2] *ExtreMe Matter Institute EMMI, GSI Helmholtzzentrum für Schwerionenforschung GmbH, 64291 Darmstadt, Germany*
[3] *Max-Planck-Institut für Astrophysik, Karl-Schwarzschild-Str. 1, 85748 Garching, Germany*
[4] *Physik Department, Technische Universität München, James-Franck-Str. 1, 85748 Garching, Germany*
[5] *Max-Planck-Institut für Kernphysik, Saupfercheckweg 1, 69117 Heidelberg, Germany*

Neutrino-pair production and annihilation through nucleon-nucleon bremsstrahlung is included in current supernova simulations by rates that are based on the one-pion-exchange approximation. Here we explore the consequences of bremsstrahlung rates based on a modern nuclear interactions for proto-neutron star cooling and the corresponding neutrino emission. We find that despite a reduction of the bremsstrahlung emission by a factor of 2–5 in the neutrinospheric region, models with the improved treatment exhibit only $\lesssim$5% changes of the neutrino luminosities and an increase of $\lesssim$0.7 MeV of the average energies of the radiated neutrino spectra, with the largest effects for the antineutrinos of all flavors and at late times. Overall, the proto-neutron star cooling evolution is slowed down modestly by $\lesssim$0.5–1 s.

I. INTRODUCTION

Neutrinos play an important role in core-collapse supernovae. Not only will they allow us to probe the interior of the next galactic supernovae, they also carry away most of the energy liberated during core collapse and deposit some of that energy in the region behind the shock, thus possibly triggering the explosion (see, e.g., [1–5] and references therein). A sound theoretical understanding of neutrino interactions is therefore a key ingredient to realistic supernova simulations.

Among the interactions involving nucleons, elastic scattering is the main source of neutrino opacity. However, this does not change the number of neutrinos nor their energy. **The neutrino energy can be changed also by inelastic scattering on interacting nucleons ($\nu NN \leftrightarrow \nu NN$), while the closely related n**ucleon-nucleon (NN) bremsstrahlung and its inverse, pair absorption, ($NN \leftrightarrow NN\nu\bar{\nu}$) play an important role both for determining the cooling of the newly formed neutron star and the neutrino spectra.

The bremsstrahlung rates used in supernova simulations are typically based on analytical fit functions provided by Hannestad and Raffelt [6] (HR) who treated the nucleon-nucleon potential in the one-pion-exchange (OPE) approximation at Born level and essentially considered the interactions among neutrons only.

Besides the bremsstrahlung rates, Hannestad and Raffelt also provided an expression for inelastic scattering, however without including recoil effects consistently in reactions on single and two nucleons. Using the HR, Refs. [7, 8] demonstrated that including energy transfers by inelastic scattering ($\nu NN \to \nu NN$) in addition to NN bremsstrahlung and neutrino-pair absorption as well as energy transfers by nucleon recoil ($\nu + N \to \nu + N$) has a negligible effect on neutrino transport results in simulations. For this reason inelastic scattering was not taken into account in the development of VERTEX, because this code considers the detailed nucleon recoil effects already. Future work will have to investigate whether these conclusions also hold for the case when inelastic scattering is included by more sophisticated calculations and when recoil effects are included consistently in reactions on single and two nucleons.

Recently, Bacca *et al.* [9, 10] studied NN bremsstrahlung using modern nuclear interactions based on chiral effective field theory (EFT) [11–14]. This was generalized to mixtures of neutrons and protons by Bartl *et al.* [15]. In addition, they demonstrated the necessity to go beyond the Born approximation at low densities and did so employing a T-matrix-based formalism using as input phase shifts extracted from experiment. For neutrons, bremsstahlung rates based on NN scattering were also developed previously by Hanhart *et al.* [16].

In this paper, we investigate the influence of the bremsstrahlung rate on the supernova and proto-neutron star evolution and the corresponding neutrino emission by comparing results with our improved treatment and the HR description, using one-dimensional simulations of a 9.6 $M_\odot$ and a 27 $M_\odot$ progenitor, producing neutron stars of about 1.25 $M_\odot$ and 1.59 $M_\odot$ (gravitational mass), respectively.

After completion of our work we became aware of a similar study by Fischer, however for an 18 $M_\odot$ progenitor star giving birth to a neutron star with a baryonic mass of 1.65 $M_\odot$ (gravitational mass of 1.45–1.5 $M_\odot$) [17]. In contrast to our hydrodynamic evolution models, the **hydrodynamic** simulations by Fischer do not include the effects of proto-neutron star convection. Nevertheless, the main conclusions from both studies are basically in agreement.

Our approach can be summarized as follows: We calculate energy-averaged mean-free paths using the T-matrix-based formalism from Ref. [15] relative to one-pion-exchange results. We use a parametrization of the temperature in terms of the density and fixed values of the electron frac-

tion to obtain a set of one-dimensional fits for this ratio as a function of density. We then implement this estimate of the improved rate in our simulations by multiplying the HR rate by this ratio.

In Sec. II we briefly discuss the bremsstrahlung rate used here and provide a simple analytical correction factor that allows **us** to rescale the standard rate based on the simple OPE ansatz. In Sec. III we describe the numerical setup of the supernova simulations. We present our results in Sec. IV mainly for simulations of one progenitor star. Finally, we conclude in Sec. V.

II. STRUCTURE FACTOR FOR BREMSSTRAHLUNG

In Ref. [15], the formalism for bremsstrahlung rates in mixtures of protons and neutrons was developed and a partial-wave decomposition of the expression was done. We will work with this expression and use NN phase shifts extracted by the Nijmegen partial-wave analysis [18] in combination with the T-matrix. At this level, the on-shell partial-wave-expanded matrix elements are given in terms of the phase shifts δ_{lSJ} by

$$T_{lSJ}(\boldsymbol{k},\boldsymbol{k};E=\frac{k^2}{\mu}) = -\frac{2\pi}{\mu}\frac{e^{2i\delta_{lSJ}}-1}{2ik} \tag{1}$$

in uncoupled and

$$T_{ll'SJ}(\boldsymbol{k},\boldsymbol{k};E=\frac{k^2}{\mu}) = -\frac{2\pi}{\mu}\frac{1}{2ik} \times \begin{cases} \left[e^{2i\delta_{lSJ}}\cos 2\epsilon_J - 1\right] & \text{for } l = l', \\ \left[ie^{i(\delta_{lSJ}+\delta_{l'SJ})}\sin 2\epsilon_J - 1\right] & \text{for } l \neq l' \end{cases} \tag{2}$$

in coupled channels. Here, $\boldsymbol{k}$ is the relative momentum and μ the reduced mass of the nucleons, l, l' and S are the orbital angular momenta and the total spin of the nucleon pair, and ϵ_J is the mixing angle for given total angular momentum J. Note that in the case of OPE, the relaxation rates can be calculated analytically by evaluating the spin traces in Ref. [15].

A. Analytical correction factor

For a first estimate of the impact that the findings in Ref. [15] have on the proto-neutron star cooling and the corresponding neutrino emission, we calculate an analytical correction factor

$$r_{Y_e}(\rho) \equiv \frac{\langle\lambda^{-1}\rangle(\rho,Y_e,T(\rho))}{\langle\lambda^{-1}\rangle_{\mathrm{OPEnn}}(\rho,T(\rho))} \tag{3}$$

of the neutrino-antineutrino annihilation opacity relative to the one-pion-exchange neutron-only (OPEnn) results, which are conceptionally similar to Hannestad and Raffelt [6]. In this first step, the correction factor is a function of density ρ only. The temperature T is parametrized by using

$$T(\rho) = T_{\mathrm{SN}}(\rho) \equiv 3\,\mathrm{MeV}\left(\frac{\rho}{10^{11}\,\mathrm{g\,cm^{-3}}}\right)^{1/3}, \tag{4}$$

which was found to represent typical conditions in simulations [10] (see also the discussion in Sec. IV) and the electron fraction Y_e is treated as a parameter that only takes fixed values (see Sec. III). The inverse mean-free path is averaged over Boltzmann distributed neutrino and antineutrino spectra. Both the T-matrix and OPEnn results are calculated using the formalism discussed in Ref. [15], which assumes nondegenerate conditions. Our results are then fitted by a function of the form

$$r_{Y_e}(\rho) = a\ln(\rho) + 10^{10}/\rho^b + c\,, \tag{5}$$

where ρ is given in $\mathrm{g\,cm^{-3}}$.

High-density rates are needed in the simulations, but beyond nuclear saturation density, neutrinos are trapped and therefore reactions are in equilibrium. In addition, our formalism breaks down at high densities. As we do not expect r to go to 0, we extrapolate our results with a constant, $r(\rho \geq \rho_0) = 0.14$, to densities beyond saturation density, $\rho_0 = 2.8\times10^{14}\,\mathrm{g\,cm^{-3}}$. While the choice is not well constrained, it is not expected to impact the simulation due to the equilibrium conditions. For three relevant Y_e values, we show the fit parameters in Table I and a comparison of our data points and fits in Fig. 1.

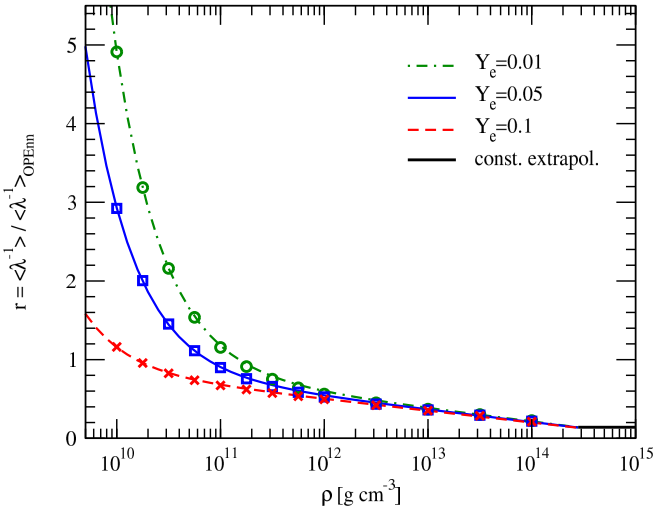

FIG. 1. Correction factor r according to Eq. (3) (symbols) and fit results (lines) for $Y_e = 0.01, 0.05,$ and 0.1 as a function of density ρ. Also shown is the constant extrapolation beyond saturation density.

B. Comparison with Hannestad and Raffelt

As mentioned in Sec. II A, we compute our T-matrix correction factor relative to the OPE nn-only rate in our

TABLE I. Fit parameters for $r(\rho)$, Eq. (5), for $Y_e = 0.01, 0.05,$ and 0.1 shown in Fig. 1.

Y_e	a	b	c
0.01	−0.0649830	1.0446877	2.2954877
0.05	−0.0685806	0.9680116	2.4176686
0.1	−0.0726502	0.9395710	2.5558616

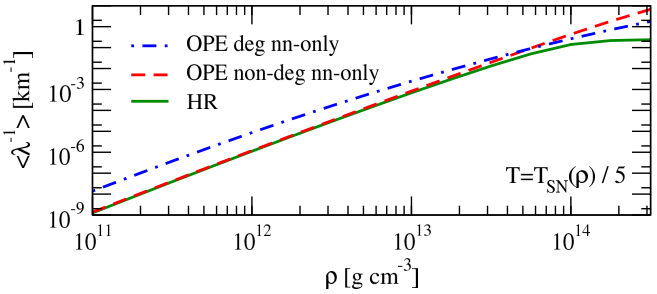

FIG. 2. Energy-averaged inverse mean-free path for pair annihilation by the bremsstrahlung process as a function of density, comparing HR results [6] with our formalism in the degenerate and non-degenerate limits. Note that the plot is based on a temperature-density relation as given by Eq. (4) but reduced by a factor of 5.

formalism, which is conceptually similar to HR (obtained in the OPE approximation and including protons as if they were neutrons). It does, however, exhibit deviations from the actual HR result especially at high densities. One possible explanation for this deviation is degeneracy. At $10^{14}\,\mathrm{g\,cm^{-3}}$, $T_{\mathrm{SN}}/T_{\mathrm{F}} \approx 1$, so degeneracy effects start to contribute. Here, the Fermi temperature T_{F} is the (neutron) Fermi energy in units of temperature. Our formalism is purely non-degenerate (but was shown in pure neutron matter to be a good approximation for partially-degenerate matter, see Ref. [10]), while the HR formalism interpolates between degenerate and non-degenerate conditions.

In order to test this explanation, we make the conditions more degenerate in Fig. 2 by reducing the temperature by a factor of 5 compared to the parametrization in Eq. (4). At low densities, HR and the non-degenerate OPE results agree very well. At $10^{14}\,\mathrm{g\,cm^{-3}}$, $T/T_{\mathrm{F}} \approx 0.2$ and deviations between these are significant. A degenerate version of our formalism is available [9, 19] which we would expect to match the HR results at lower T/T_{F}. The opacity obtained with this structure factor is also shown in Fig. 2. While it lies closer to the HR opacity at high densities, there is still a significant deviation. The HR opacity levels off and would eventually decrease if we increase the density even further. This maximum can be moved to lower densities by making the conditions even more degenerate. The handling of multiple-scattering effects in the HR formalism seems to be the root of this maximum, which we consider to be likely unphysical as a denser medium should always be more opaque.

Using the comparison with OPE nn-only results has the advantage that the assumptions and approximations of the formalism are the same and our correction factor directly measures the impact of the more advanced nuclear interactions compared to OPE. As our correction factor is a crude approximation by construction, this strategy seems justified.

III. NUMERICAL SETUP AND SIMULATED MODELS

Our simulations were performed with the one-dimensional version of the Prometheus-Vertex code [20], i.e., in spherical symmetry. We use the most elaborate set of neutrino processes as described in Ref. [20] with the improvements of Ref. [21] and further upgrades as reported in Ref. [22]. In particular, our revised implementation of charged-current neutrino-nucleon interactions (according to Ref. [23]) includes nucleon self-energy corrections [24–27]. We also account for differences in the weak-magnetism corrections of neutral-current neutrino-nucleon scatterings as in Ref. [28] by a separate treatment of the transport of $\nu_{\mu,\tau}$ and of $\bar{\nu}_{\mu,\tau}$. Moreover, we take into account proto-neutron star convection by a mixing-length treatment as described in Ref. [22].

The T-matrix modified bremsstrahlung rates are implemented using the fit formula of Eq. (5) with the parameter values of Table I to correct the HR rates employed in our standard description. To handle the Y_e dependence of the coarsely gridded table data a step function in Y_e space is used. Specifically, for grid cells with $Y_e < 0.05$ the tabulated fit for $Y_{e,\mathrm{table}} = 0.01$ is applied, for grid cells with $0.05 \leq Y_e < 0.1$ the tabulated fit for $Y_{e,\mathrm{table}} = 0.05$, and finally for grid cells with $Y_e \geq 0.1$ the tabulated fit for $Y_{e,\mathrm{table}} = 0.1$ is adopted. This allows us to always test the maximal influence of the T-matrix correction factor in the low-density regime of $\rho < 10^{11}\,\mathrm{g\,cm^{-3}}$ as the strength of the correction decreases with increasing Y_e, see Fig. 1. Conversely, for high-density proto-neutron star conditions of $\rho > 10^{12}\,\mathrm{g\,cm^{-3}}$, where bremsstrahlung is most relevant, the correction factors are nearly independent of Y_e and the details of the handling of the tabulated data are less important. The chosen Y_e correction factor is then applied to the 0th and 1st Legendre moments of the bremsstrahlung opacities in an energy-independent way, because the correction factors are given as ratios of the annihilation opacities for neutrino and antineutrino pairs populating equilibrium phase-space distributions. **Since bremsstrahlung annihilation and $\nu\bar{\nu}$ pair production are implemented by applying detailed-balance constraints, neutrino equilibration is guaranteed to be numerically recovered.**

We simulate the phases of stellar core-collapse, bounce, post-bounce accretion and supernova explosion, and the subsequent cooling of the proto-neutron star for up to more than 10 s for a $9.6\,M_{\odot}$ progenitor star (see Refs. [29–

31]) and a $27\,M_\odot$ progenitor (see Ref. [32]). In the former simulation, we employ the SFHo equation of state (EOS) for hot nuclear matter of Ref. [33], in the latter case the LS220 EOS of Lattimer and Swesty [34] with incompressibility $K = 220\,\mathrm{MeV}$. Results of our simulations using the standard implementation of NN bremsstrahlung according to the HR rates [6] were reported in Ref. [22].

While the $9.6\,M_\odot$ model as a low-mass progenitor with very steep density gradient outside of the iron core explodes naturally even in spherical symmetry [31], the explosion of the $27\,M_\odot$ model is initiated artificially at 0.5 s after core bounce by reducing the pre-shock density and thus the explosion-damping mass-accretion rate of the stalled shock gradually by up to a factor of 30 (see also Ref. [22]).

IV. RESULTS

A. Post-processing opacities

Before discussing the impact of the correction factor on the proto-neutron star cooling and neutrino emission, we evaluate the quality of our approximation by post-processing the radial profiles obtained in the simulation of the $27\,M_\odot$ progenitor and comparing the corrected HR results with the full T-matrix results.

We do so in Fig. 3, where we show the inverse mean-free path for a neutrino with $E = \langle E_{\nu_x} \rangle$ against pair annihilation, assuming a Fermi-Dirac distribution for the antineutrino. Here, $\langle E_{\nu_x} \rangle$ is the local mean neutrino energy of muon/tau neutrinos as obtained in the simulation. The plot range is determined by the radius where the density drops below $10^{10}\,\mathrm{g\,cm^{-3}}$. The ν_x neutrinosphere position is indicated by the green vertical line. We define it by the radius where the optical depth of a neutrino with local mean energy becomes smaller than one, using the sum of the opacities of all kinds of (in)elastic scattering and pair annihilation processes (averaged for muon and tau neutrinos). This location roughly marks the region where neutrinos decouple from the stellar medium, but it is neither identical with the energy sphere nor with the transport sphere [7, 35], which have to be introduced for a detailed discussion of muon and tau neutrino transport. The densities corresponding to the neutrinospheric positions according to our (crude) definition can be extracted from Fig. 4, where we present density profiles of the proto-neutron star corresponding to the times picked for Fig. 3.

Ideally, the blue lines showing the approximated and full T-matrix result should lie on top of each other. Looking at the earlier profiles up to 1 s, we find good agreement between the two lines over a wide density range and especially around the neutrinosphere where the rates are most relevant.

We do find deviations, however, at small and large radii. The former can be attributed to degeneracy effects, which are neither included in our non-degenerate T-matrix formalism nor in the OPEnn calculations used to fit the correction factor, but they are taken into account by the HR rate. The black solid lines show the ratio of the temperature over the Fermi temperature, T/T_F, as an indicator of the degeneracy. (T_F is the Fermi energy divided by the Boltzmann constant.) Deviations appear where this value is significantly below 1. No formalism has been derived yet to calculate bremsstrahlung rates in mixtures of neutrons and protons at degenerate conditions using modern interactions. Nevertheless, we can use the formalism developed in Refs. [9, 19] to calculate T-matrix opacities in pure neutron matter under degenerate conditions (in the region where $T/T_\mathrm{F} < 1/\pi$). This can explain some of the discrepancy, but the original HR result still lies closer to the T-matrix opacities than the corrected one. This is partly a result of the HR issues discussed in Sec. II B.

The deviations found at small densities in the outer regions can be attributed to temperature effects. Our fit factor is a one-dimensional function of density, assuming temperature to be parametrized by $T_\mathrm{SN}(\rho)$ given by Eq. (4). We plot T/T_SN along the profiles in Figure 3 and see significant deviations from unity especially in the core and at large radii.

At later times, the proto-neutron star has cooled and becomes highly degenerate. In the outer regions, our approximation still works fine, while in the center degeneracy effects lead to major deviations between our non-degenerate T-matrix results and the corrected HR opacities. As expected, this is significantly reduced when using the degenerate T-matrix rate instead. However, the discrepancies remain sizable.

Since neutrinos are in equilibrium in the high-density regions of the proto-neutron star interior and free-streaming in the low-density outer regions, the intermediate region around the neutrinosphere is most important for both the proto-neutron star cooling and the neutrino signal. In this region, our approximation works reasonably well, except for very late times when the neutrinospheres lie inside the degenerate proto-neutron star.

Furthermore, our corrected HR result tends to overestimate the effects. Hence our first sensitivity study can be considered as a test for the upper bounds on consequences of T-matrix modifications to the bremsstrahlung process.

B. Impact on proto-neutron star cooling and neutrino emission

As mentioned in Sec. III, we have simulated the collapse and explosion as well as the subsequent proto-neutron star cooling phase for a $9.6\,M_\odot$ and a $27\,M_\odot$ progenitor.

The investigated $9.6\,M_\odot$ progenitor can explode fairly easily and rapidly by the neutrino-driven mechanism even in spherical symmetry [22, 36], whereas explosions of progenitors above $\sim 10\,M_\odot$ (like the $27\,M_\odot$ case sim-

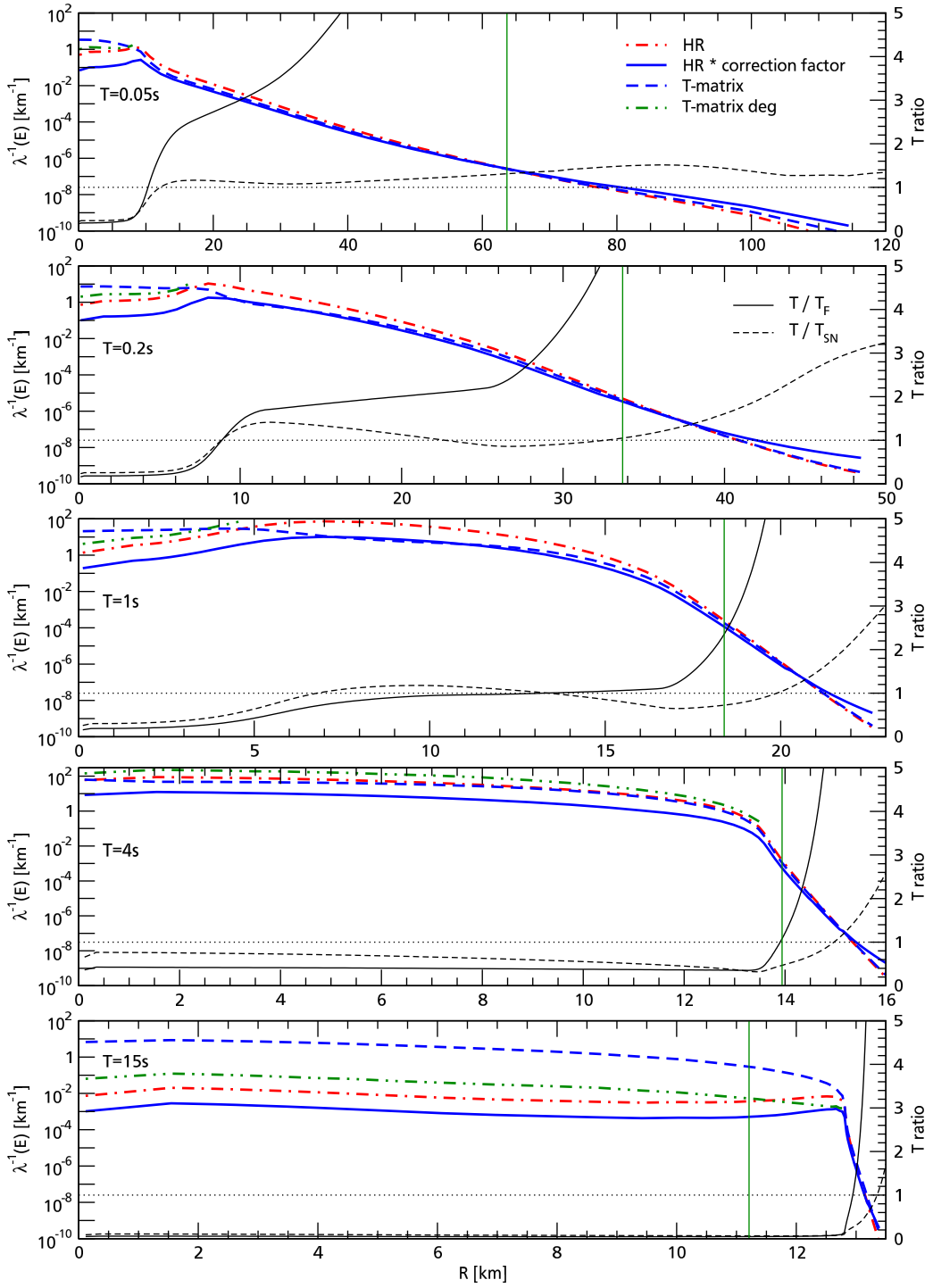

FIG. 3. Inverse mean-free path against pair absorption for a ν_x with local mean energy as a function of radius along profiles for our 27 $M_\odot$ simulation at 50 ms, 200 ms, 1 s, 4 s, and 15 s. Shown is the opacity used in the simulation (HR × correction factor, blue solid line) along with the HR (red dash-dotted line) and T-matrix (blue dashed line) opacities. For comparison, we also show degenerate T-matrix results calculated for pure neutron matter. The black solid line shows the degeneracy $T/T_{\rm F}$, the black dashed line shows $T/T_{\rm SN}$ [see Eq. (4)]. The green vertical line indicates the position of the ν_x neutrinosphere.

ulated here) require the support by multi-dimensional effects and in spherically symmetric simulations (such as the ones performed in this work) need to be triggered artificially. In all cases, however, including the 9.6 $M_\odot$ star, multi-dimensional effects have a strong influence on how and when the explosion develops. For this reason it does

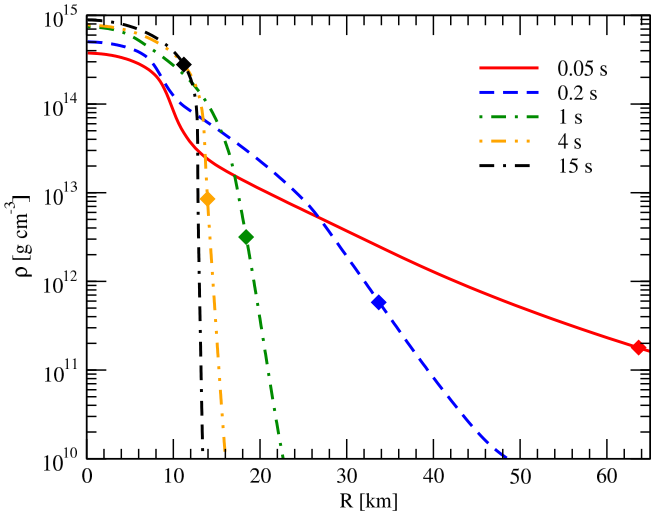

FIG. 4. Density versus radius of the proto-neutron star in our $27\,M_\odot$ model at the times displayed in Fig. 3. The colored **diamonds** mark the position of the ν_x neutrinosphere (as also shown in Fig. 3).

not make any sense to discuss possible effects of a modified treatment of the bremsstrahlung process on the explosion mechanism on the basis of spherically symmetric simulations. We therefore constrain our discussion here mostly on the differences caused by the bremsstrahlung process during the proto-neutron star cooling phase.

The most important consequence of the effective T-matrix rates [i.e., of the HR rates multiplied by the correction factor of Eqs. (3) and (5)] is to reduce the annihilation opacity of the bremsstrahlung process for neutrino pairs inside of the nascent neutron star. This can be concluded from Fig. 1, where the correction factor drops below unity at densities above $\sim 10^{11}\,\mathrm{g\,cm^{-3}}$, which is (roughly) interior to the neutrinosphere of ν_e. Correspondingly, also the production rate of neutrino-antineutrino pairs through this reaction is decreased, affecting mainly the emission of heavy-lepton neutrinos (ν_x), which are not created by charged-current processes in the absence of muons and tau leptons [8]. With the T-matrix rates, we therefore expect a reduced emission of muon and tau neutrinos and a corresponding delay of the cooling of the newly formed neutron star.

This expectation is confirmed by Fig. 5, which shows that **for both progenitor models** the new-born neutron star becomes slightly hotter in the innermost core but also cools more slowly, i.e., the temperature remains higher for a longer time. It is important to note that this evolution difference of the cooling proto-neutron star is initially triggered by the reduced production of $\nu_x\bar{\nu}_x$ pairs via the effective T-matrix rates in the neutrino-decoupling layers near the neutron-star surface, but not by a change of the diffusion time scale of neutrinos out of the dense interior of the neutron star. The diffusion time scale is hardly affected by the modification of the bremsstrahlung rate, because the total opacity is largely dominated by neutral-current neutrino-nucleon scatterings and neutrino annihilation by bremsstrahlung contributes only at a minor level.

In agreement with this we observe very small differences of the radiated neutrino luminosities and mean energies (Figs. 6 **and 7**) during the accretion phase before the explosion is artificially initiated at 0.5 s after core bounce. During this phase the neutrino emission is mainly produced in the hot accretion mantle, where $e^\pm$ and $\nu_e\bar{\nu}_e$ annihilation dominate the $\nu_x\bar{\nu}_x$ production. Only after accretion has ended (when the explosion is well on its way, $t \gtrsim 0.8\,\mathrm{s}$ after bounce), the ν_x and $\bar{\nu}_x$ emission is significantly enhanced by the generation of these neutrinos through the bremsstrahlung process, which dominates in the denser regions to which the ν_x neutrinosphere retreats. Consequently, the differences of the radiated neutrino luminosities and mean energies between the runs with HR and T-matrix rates begin to grow gradually and become largest at late times.

In detail, **for the** $27\,M_\odot$ **progenitor** we observe a slight reduction of the luminosities of $\nu_{\mu,\tau}$ and $\bar{\nu}_{\mu,\tau}$ with the T-matrix rates (Fig. 6), while the radiated mean energies of these neutrinos are larger by up to $\sim$0.5 MeV with the biggest effects at late times and slightly bigger for the antineutrinos (Fig. 6), which (due to the weak-magnetism corrections) have lower nucleon-scattering opacities and

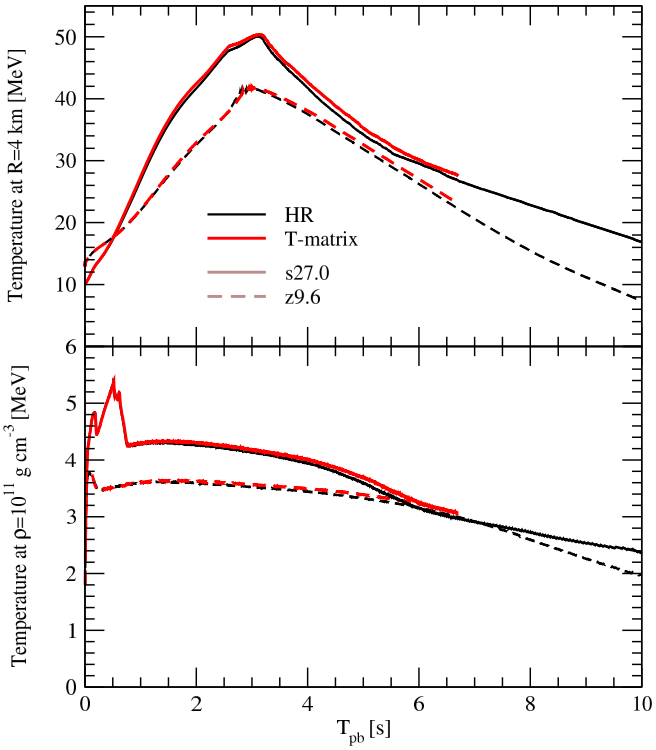

FIG. 5. **Temperature in MeV in the innermost core of the nascent neutron star (at a radius of 4 km; top panel) and at a density of $10^{11}\,\mathrm{g\,cm^{-3}}$ (bottom panel) in our $27\,M_\odot$ (solid lines) and $9.6\,M_\odot$ (dashed lines) models as functions of time after bounce.**

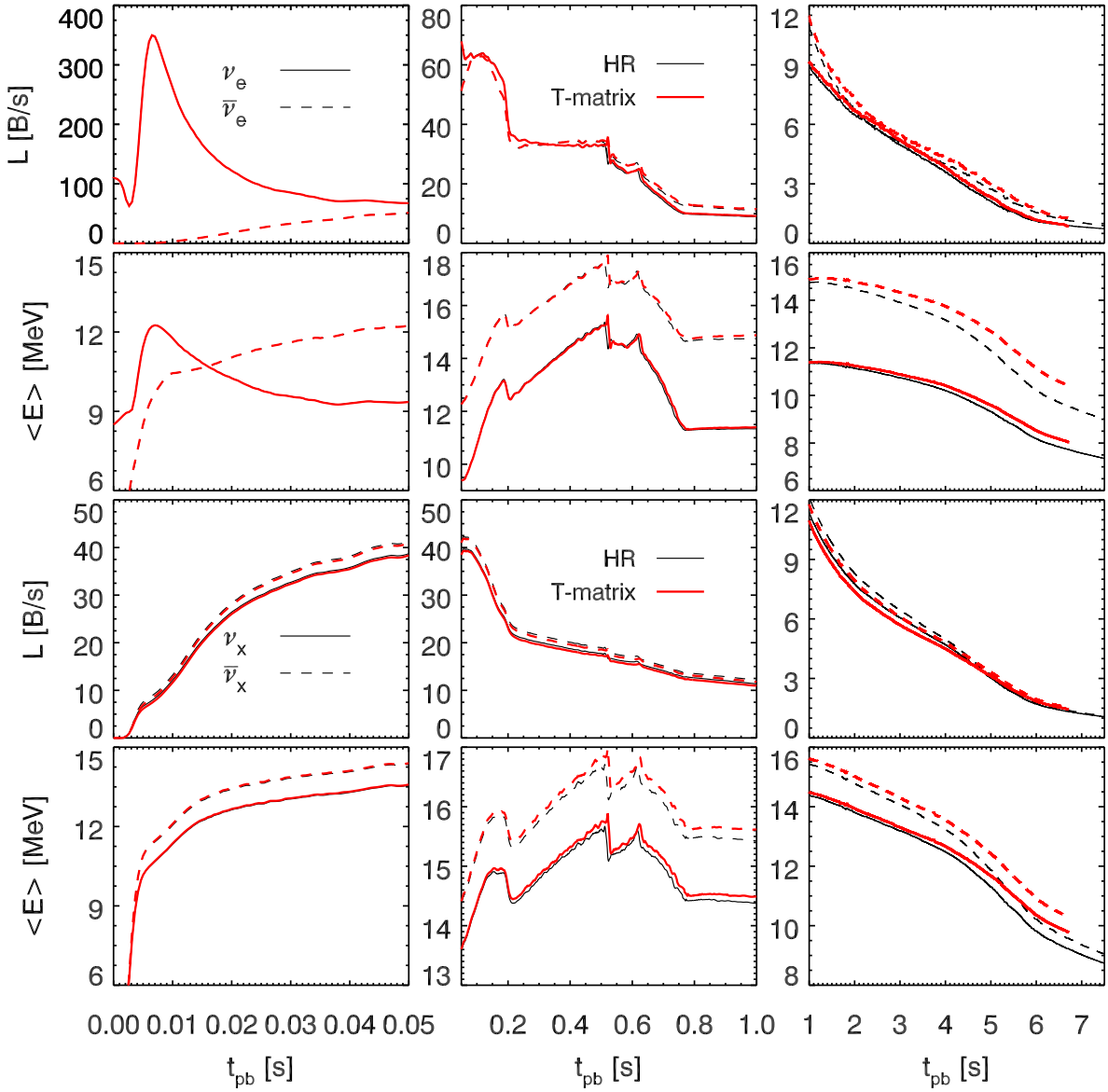

FIG. 6. Neutrino luminosities (in $10^{51}\,\mathrm{erg\,s^{-1}}$; bethe/s or B/s) and radiated mean neutrino energies for our $27\,M_\odot$ simulation as function of time after bounce, evaluated at a radius of 500 km for an observer in the lab frame at infinity. The left column shows the shock-breakout and ν_e burst phase, the middle column the accretion phase with the onset of the supernova explosion, and the right column the neutrino signal during the Kelvin-Helmholtz cooling phase of the newly formed neutron star. The upper two rows provide the luminosities and mean energies for ν_e and $\bar{\nu}_e$, the lower two rows those for heavy-lepton neutrinos, ν_x, and antineutrinos, $\bar{\nu}_x$.

decouple at a deeper energy sphere. These observations are compatible with the decreased $\nu_x\bar{\nu}_x$ production by the T-matrix bremsstrahlung rate, which moves the energy spheres of these neutrinos to higher temperatures. On a much smaller level these effects can be observed also during the accretion phase.

The ν_e and $\bar{\nu}_e$ emission properties exhibit hardly any differences dependent on the bremsstrahlung treatment during the accretion phase, where their emission originates from a neutrinospheric region that is located within the hot accretion layer. Only after accretion has ended ($t \gtrsim 0.8\,\mathrm{s}$) differences appear and grow gradually. Figure 6 shows that the T-matrix case, because of higher temperatures in the core of the proto-neutron star as well as in its outer regions (Fig. 5), leads to an increase of the radiated ν_e and $\bar{\nu}_e$ luminosities by up to $\sim$4% at $t \gtrsim 1\,\mathrm{s}$ after bounce. Electron neutrinos and antineutrinos therefore take over some of the energy transport from the flux-reduced heavy-lepton neutrinos. Simultaneously, the mean energies of ν_e and $\bar{\nu}_e$ increase by up to $\sim$0.7 MeV with the bigger differences for $\bar{\nu}_e$ and at later times. These differences lead to an enhancement of the loss of ν_e number relative to the loss of $\bar{\nu}_e$, accelerating the deleptonization of the nascent neutron star. This explains the

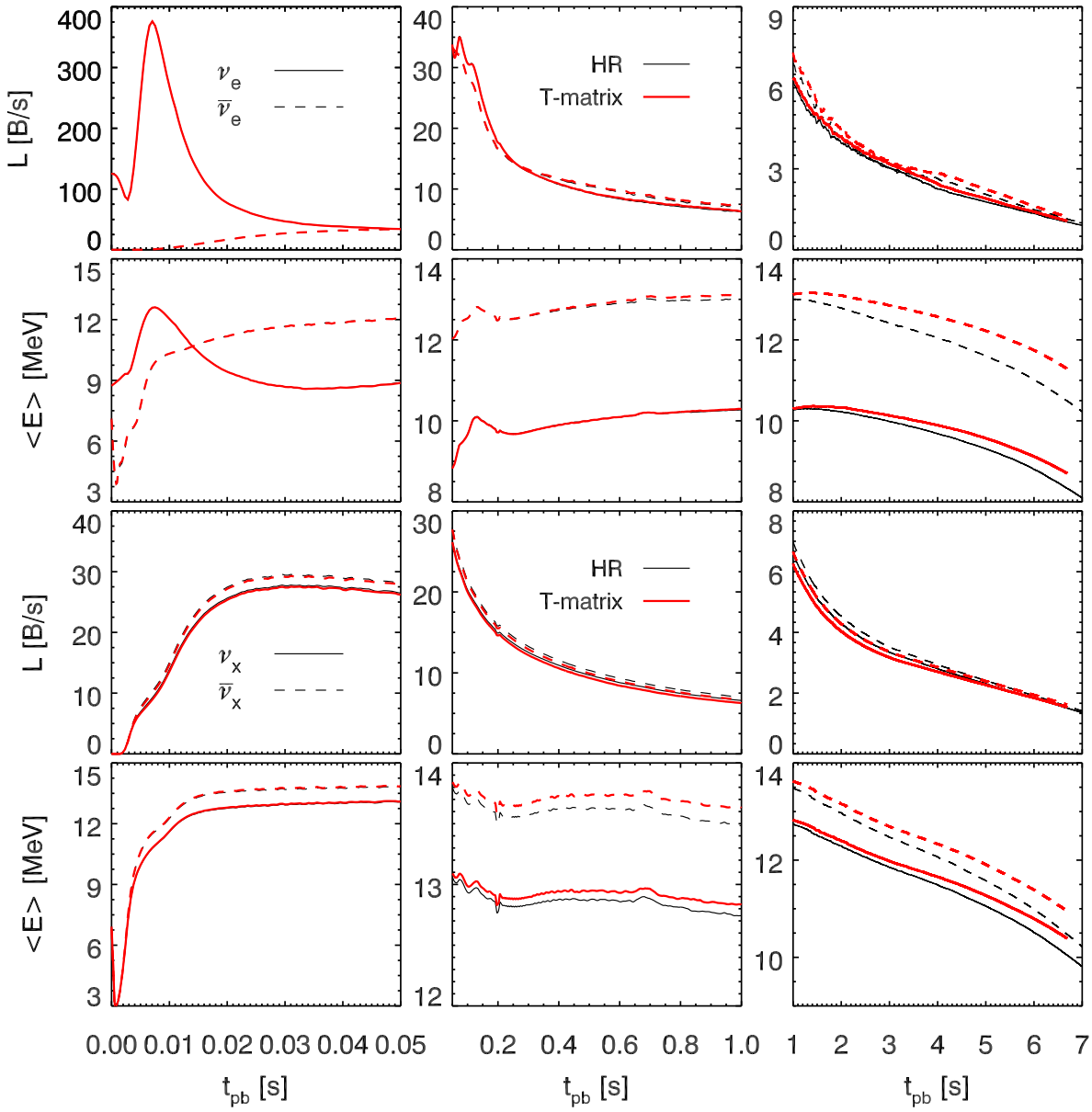

FIG. 7. **Same as Fig. 6, but for the** $9.6\,M_\odot$ **simulation**

higher inner-core temperatures seen in Fig. 5 by resistive heating (converting degeneracy energy of electrons to thermal energy by down-scattering [37]). At the same time the total neutrino luminosity (i.e., the sum of the luminosities of all neutrino species) is decreased and the proto-neutron star cooling takes correspondingly longer. The growing differences of the neutrino emission at late times therefore are not directly caused by the instantaneous differences of the bremsstrahlung rates of the HR and T-matrix calculations. Instead, they mainly reflect the differences of the neutron-star temperature and lepton-number profiles, which diverge more and more as time goes on and as the time-integrated effects of different bremsstrahlung treatments accumulate.

While we have displayed and discussed the results of our simulations for the $27\,M_\odot$ progenitor, which gives birth to a neutron star with $\sim$1.776 ($\sim$1.592) $M_\odot$ baryonic (final gravitational) mass [22], the differences in the bremsstrahlung rates were found to have very similar effects in the case of the $9.6\,M_\odot$ star, whose explosion leaves behind a neutron star with a baryonic (gravitational) mass of $\sim$1.363 (1.252) $M_\odot$**, see Fig. 7**. Overall, the luminosity decline of ν_e and $\bar{\nu}_e$ is delayed with the T-matrix rates by at most a few 100 ms, whereas the mean energies of $\bar{\nu}_e$ decrease to the same cooling level at late times only with a delay of up to $\sim$1 s.

V. CONCLUSIONS

We have explored the impact of new T-matrix results for NN bremsstrahlung in mixtures of neutrons and protons from Ref. [15] in simulations of core-collapse supernovae. Comparing the T-matrix results to the standard HR rate [6], we have developed a simple correction factor as a function of density that can be used in simulations. This allowed for a first estimate of how bremsstrahlung rates with modern nuclear interactions have an impact on the cooling evolution and neutrino emission of newly formed, hot neutron stars. Our approximation is constructed such that it tends to produce upper bounds on the possible changes compared to the case using the HR bremsstrahlung rate.

Because of the lack of charged-current production by beta-reactions with nucleons in the absence of muons and tauons, neutrino-antineutrino pair production and annihilation by the bremsstrahlung process affects mostly the transport of heavy-lepton neutrinos, ν_x, in the supernova core and in newly formed neutron stars. Any corresponding effect on the transport and emission of ν_e and $\bar{\nu}_e$ is only indirect through changes of the dynamical and thermal evolution of the nascent neutron star as a consequence of alterations of the ν_x transport. An exception to this fact may be the emission of $\bar{\nu}_e$ at very late times, when the medium of the proto-neutron star becomes progressively neutron-dominated and degenerate, in which case the production of $\bar{\nu}_e$ by beta-reactions diminishes and bremsstrahlung becomes relatively more important also for $\bar{\nu}_e$.

The differences in the neutrino emission for our modified bremsstrahlung treatment compared to the HR rate show up mainly after the post-bounce accretion has ended due to the onset of the supernova explosion, i.e., during the Kelvin-Helmholtz cooling of the new-born neutron star. Our calculations imply a reduction of the bremsstrahlung rate to ∼60–20% of the reference case based on the HR rate in the density regime between $\sim 10^{12}\,\mathrm{g\,cm^{-3}}$ and $\sim 10^{14}\,\mathrm{g\,cm^{-3}}$ (Fig. 1), where the ν_x neutrinospheres are located during most of the cooling evolution of the compact remnant (Fig. 4).

With this reduction we find a modest stretching of the neutrino-cooling time (by ∼0.5–1 s) of the nascent neutron star. Because of the reduced production of heavy-lepton neutrinos, the ν_x luminosities decrease by up to ∼5%, whereas higher temperatures in the neutron star lead to an increase of the ν_e and $\bar{\nu}_e$ luminosities also by a few percent. The hotter neutron star emits all neutrino species with slightly harder spectra. The biggest effect can be seen for $\bar{\nu}_e$ and $\bar{\nu}_x$, whose mean energies of the radiated spectra are higher by up to more than 0.5 MeV at late times. The differences of the neutrino-emission properties between both bremsstrahlung treatments grow with time. This is mainly a consequence of the accumulating differences in the thermal structure of the neutron stars due to their divergent evolution, and it is less caused by larger instantaneous differences of the bremsstrahlung rates in the late (more degenerate) stages.

Despite the slightly higher mean energies of the radiated $\bar{\nu}_e$, the neutrino-driven baryonic wind of the nascent neutron stars exhibits an insignificantly lower (by $\lesssim$0.01) electron (proton) fraction and remains proton-rich at all times as reported in Ref. [22], which disfavors r-process nucleosynthesis in the wind ejecta. A similarly weak impact of the different treatments of NN bremsstrahlung on the characteristics of the neutrino-driven wind was also reported from the independent study by Fischer [17], who observed a reduction of the wind-Y_e by at most ∼0.004. This is compatible with our findings, although the time evolution of this outflow property differs considerably from the one obtained in our simulations. Because of the omission of convection inside the newly formed neutron star, the wind ejecta in Fischer's models evolve from slightly proton-rich to slightly neutron-rich conditions within a fraction of a second to dive through a flat minimum between 2 and 3 seconds and to continuously increase subsequently. In contrast, including convection in our proto-neutron star cooling calculations accelerates the neutronization of the compact remnant. Therefore the wind-Y_e in our models is on the proton-rich side all the time and evolves through a broad hump of several seconds duration, corresponding to the main period of deleptonization, before it joins the late-time trend of a monotonic rise seen in Fischer's simulations (the reader is referred to the discussion of this behavior in Ref. [22]).

One may wonder why a reduction of the bremsstrahlung rates by factors of 2–5 in the relevant region around the neutrinospheres does not have a stronger impact on the cooling history and neutrino emission. The reason for this modest reaction are compensating effects, which are very typical of the considered multi-component system with its tightly and nonlinearly coupled ingredients, whose response to variations can damp and balance consequences of changes of individual ingredients. In the considered case, the increasing temperatures in the neutron star for reduced bremsstrahlung lead to more $\nu_x\bar{\nu}_x$ creation by $e^{\pm}$ and $\nu_e\bar{\nu}_e$ pair annihilation (with an energy production rate rocketing with $\sim T^9$) so that these latter processes nearly completely compensate the decrease of the emission by the bremsstrahlung process. We also point out that changes of the bremsstrahlung rate below a density of $\sim 10^{11}\,\mathrm{g\,cm^{-3}}$ have hardly any influence, because at such low densities neutrinos begin to possess very large mean free paths and therefore make the transition to free streaming. On the other side, at densities above nuclear saturation density modifications of the bremsstrahlung rate also have little influence because at such densities neutrinos are in chemical equilibrium nearly until the end of the optically thick neutrino-cooling evolution. The equilibration is achieved also by other processes like $e^{\pm}$ annihilation and the plasmon-neutrino process, and the exact time scale to establish this equilibrium is not relevant as long as it is much shorter than the evolution time scales for contraction, cooling, and

deleptonization of the nascent neutron star. Since neutral-current neutrino-nucleon scattering dominates the total neutrino opacity by far, the minor contributions from bremsstrahlung annihilation (and possible changes) also have hardly an effect on the diffusion time scale of neutrinos out of the neutron star.

In Ref. [15], calculations based on chiral EFT interactions at next-to-next-to-next-to-leading order were shown to produce results very similar to the T-matrix rates at the densities found to be relevant in this paper. Hence, we expect our conclusions to hold for chiral EFT interactions as well. This is of particular interest, as chiral EFT interactions can be used to calculate and constrain the EOS (for recent work, see Refs. [38–43]), eventually allowing for a consistent treatment of neutrino interactions and the EOS.

For a more consistent treatment of bremsstrahlung than in these explorative supernova and proto-neutron star cooling simulations, the temperature dependence of the rates has to be taken into account explicitly. In this case, a simple correction factor like the one used in our work cannot be defined as easily, but tabulated structure factors may be preferable. In addition, an interpolation is required between our non-degenerate and degenerate formalisms, and the latter needs to be extended to mixtures of neutrons protons.

ACKNOWLEDGMENTS

We thank Almudena Arcones, Lorenz Hüdepohl, Andreas Marek, Hannah Yasin, and especially Bernhard Müller, who contributed to the original implementations of nucleon self-energy corrections and of the mixing-length treatment of proto-neutron star convection in Prometheus-Vertex. This work was supported by the Deutsche Forschungsgemeinschaft through Grant SFB 1245 and the Cluster of Excellence EXC 153 "Origin and Structure of the Universe" (http://www.universe-cluster.de), the European Research Council AdG No. 341157-COCO2CASA and Grant No. 307986 STRONGINT, as well as the Studienstiftung des Deutschen Volkes. The numerical simulations were carried out on the IBM iDataPlex system *hydra* of the Max Planck Computing and Data Facility (MPCDF). We also thank the Department of Energy's Institute for Nuclear Theory at the University of Washington for its hospitality and the Department of Energy for partial support during the completion of this work.

[1] H.-T. Janka, K. Langanke, A. Marek, G. Martínez-Pinedo, and B. Müller, Phys. Rept. **442**, 38 (2007).
[2] H.-T. Janka, Annu. Rev. Nucl. Part. Sci. **62**, 407 (2012).
[3] A. Burrows, Rev. Mod. Phys. **85**, 245 (2013).
[4] T. Foglizzo *et al.*, Publications of the Astronomical Society of Australia **32**, e009 (2015).
[5] H.-T. Janka, T. Melson, and A. Summa, arxiv:1602.05576.
[6] S. Hannestad and G. Raffelt, Astrophys. J. **507**, 339 (1998).
[7] G. G. Raffelt, Astrophys. J. **561**, 890 (2001).
[8] M. T. Keil, G. G. Raffelt, and H.-T. Janka, Astrophys. J. **590**, 971 (2003).
[9] S. Bacca, K. Hally, C. J. Pethick, and A. Schwenk, Phys. Rev. C **80**, 032802 (2009).
[10] S. Bacca, K. Hally, M. Liebendörfer, A. Perego, C. J. Pethick, and A. Schwenk, Astrophys. J. **758**, 34 (2012).
[11] S. Weinberg, Phys. Lett. B **251**, 288 (1990).
[12] S. Weinberg, Nucl. Phys. B **363**, 3 (1991).
[13] E. Epelbaum, H.-W. Hammer, and U.-G. Meißner, Rev. Mod. Phys. **81**, 1773 (2009).
[14] R. Machleidt and D. R. Entem, Phys. Rept. **503**, 1 (2011).
[15] A. Bartl, C. J. Pethick, and A. Schwenk, Phys. Rev. Lett. **113**, 081101 (2014).
[16] C. Hanhart, D. R. Phillips, and S. Reddy, Phys. Lett. B **499**, 9 (2001).
[17] T. Fischer, arXiv:1608.05004.
[18] V. G. J. Stoks, R. A. M. Klomp, M. C. M. Rentmeester, and J. J. de Swart, Phys. Rev. C **48**, 792 (1993), `http://nn-online.org`.
[19] G. I. Lykasov, C. J. Pethick, and A. Schwenk, Phys. Rev. C **78**, 045803 (2008).
[20] M. Rampp and H.-T. Janka, Astron. Astrophys. **396**, 361 (2002).
[21] R. Buras, M. Rampp, H.-T. Janka, and K. Kifonidis, Astron. Astrophys. **447**, 1049 (2006).
[22] A. Mirizzi, I. Tamborra, H.-T. Janka, N. Saviano, K. Scholberg, R. Bollig, L. Hüdepohl, and S. Chakraborty, Riv. Nuovo Cim. **39**, 1 (2016).
[23] A. Burrows and R. F. Sawyer, Phys. Rev. C **58**, 554 (1998).
[24] G. Martínez-Pinedo, T. Fischer, A. Lohs, and L. Huther, Phys. Rev. Lett. **109**, 251104 (2012).
[25] L. F. Roberts, S. Reddy, and G. Shen, Phys. Rev. C **86**, 065803 (2012).
[26] S. Reddy, M. Prakash, and J. M. Lattimer, Phys. Rev. D **58**, 013009 (1998).
[27] M. Hempel, Phys. Rev. C **91**, 055807 (2015).
[28] C. J. Horowitz, Phys. Rev. D **65**, 043001 (2002).
[29] S. E. Woosley and A. Heger, Astrophys. J. **810**, 34 (2015).
[30] B. Müller, H.-T. Janka, and A. Heger, Astrophys. J. **761**, 72 (2012).
[31] T. Melson, H.-T. Janka, and A. Marek, Astrophys. J. Lett. **801**, L24 (2015).
[32] S. E. Woosley, A. Heger, and T. A. Weaver, Rev. Mod. Phys. **74**, 1015 (2002).
[33] A. W. Steiner, M. Hempel, and T. Fischer, Astrophys. J. **774**, 17 (2013).
[34] J. M. Lattimer and F. D. Swesty, Nucl. Phys. A **535**, 331 (1991).
[35] H. T. Janka, Astropart. Phys. **3**, 377 (1995).
[36] T. Melson, H.-T. Janka, and A. Marek, Astrophys. J.

801, L24 (2015).
[37] A. Burrows and J. M. Lattimer, Astrophys. J. **307**, 178 (1986).
[38] K. Hebeler, J. M. Lattimer, C. J. Pethick, and A. Schwenk, Astrophys. J. **773**, 11 (2013).
[39] T. Krüger, I. Tews, K. Hebeler, and A. Schwenk, Phys. Rev. C **88**, 025802 (2013).
[40] J. W. Holt, N. Kaiser, and W. Weise, Prog. Part. Nucl. Phys. **73**, 35 (2013).
[41] A. Carbone, A. Rios, and A. Polls, Phys. Rev. C **88**, 044302 (2013).
[42] C. Wellenhofer, J. W. Holt, and N. Kaiser, Phys. Rev. C **92** (2015).
[43] C. Drischler, K. Hebeler, and A. Schwenk, Phys. Rev. C **93**, 054314 (2016).